Since January 2020 Elsevier has created a COVID-19 resource centre with free information in English and Mandarin on the novel coronavirus COVID-19. The COVID-19 resource centre is hosted on Elsevier Connect, the company's public news and information website.

Analytica Chimica Acta 1206 (2022) 339777

Contents lists available at ScienceDirect

Analytica Chimica Acta

journal homepage: www.elsevier.com/locate/aca

Evaluation of electropolymerized molecularly imprinted polymers (E-MIPs) on disposable electrodes for detection of SARS-CoV-2 in saliva

H.F. EL Sharif [a], S.R. Dennison [b], M. Tully [c], S. Crossley [c], W. Mwangi [c], D. Bailey [c], S.P. Graham [c], S.M. Reddy [a, *]

[a] Department of Chemistry, UCLan Centre for Smart Materials, School of Natural Sciences, University of Central Lancashire, Preston, PR1 2HE, United Kingdom
[b] School of Pharmacy and Biomedical Sciences, University of Central Lancashire, Preston, PR1 2HE, United Kingdom
[c] The Pirbright Institute, Pirbright, Woking, Surrey, GU24 0NF, United Kingdom

HIGHLIGHTS

- Electropolymerized molecular imprinting approach for SARS-CoV-2 detection in saliva.
- Rapid electrochemical analysis for fast readout <10 min.
- Disposable and cost-effective sensor platform.
- Qualitative and quantitative analysis using PCA integration.
- SARS-CoV-2 specific monoclonal antibody confirmation in real patient saliva samples.

GRAPHICAL ABSTRACT

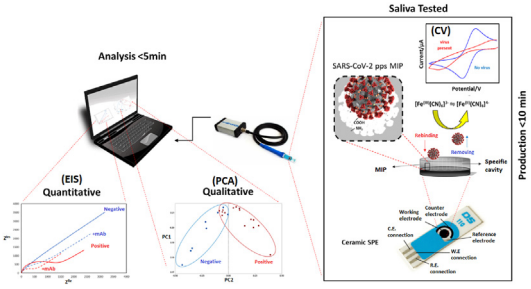

ARTICLE INFO

Article history:
Received 21 January 2022
Received in revised form
18 March 2022
Accepted 25 March 2022
Available online 1 April 2022

Keywords:
SARS-CoV-2
COVID-19
Molecularly imprinted polymers
Electrochemical polymerization
Biosensor
Electrochemical impedance spectroscopy

ABSTRACT

We investigate electropolymerized molecularly imprinted polymers (E-MIPs) for the selective recognition of SARS-CoV-2 whole virus. E-MIPs imprinted with SARS-CoV-2 pseudoparticles (pps) were electrochemically deposited onto screen printed electrodes by reductive electropolymerization, using the water-soluble *N*-hydroxmethylacrylamide (NHMA) as functional monomer and crosslinked with *N,N′*-methylenebisacrylamide (MBAm). E-MIPs for SARS-CoV-2 showed selectivity for template SARS-CoV-2 pps, with an imprinting factor of 3:1, and specificity (significance = 0.06) when cross-reacted with other respiratory viruses. E-MIPs detected the presence of SARS-CoV-2 pps in <10 min with a limit of detection of 4.9 $\log_{10}$ pfu/mL, suggesting their suitability for detection of SARS-CoV-2 with minimal sample preparation. Using electrochemical impedance spectroscopy (EIS) and principal component analysis (PCA), the capture of SARS-CoV-2 from real patient saliva samples was also evaluated. Fifteen confirmed COVID-19 positive and nine COVID-19 negative saliva samples were compared against the established loop-mediated isothermal nucleic acid amplification (LAMP) technique used by the UK National Health Service. EIS data demonstrated a PCA discrimination between positive and negative LAMP samples. A threshold real impedance signal (Z^{Re}) $\gg$ 4000 Ω and a corresponding charge transfer resistance (R_{CT}) $\gg$ 6000 Ω was indicative of absence of virus (COVID-19 negative) in agreement with values obtained for our control non-imprinted polymer control. A Z^{Re} at or below a threshold value of 600 Ω with a corresponding R_{CT} of <1200 Ω was indicative of a COVID-19 positive sample. The presence of virus was confirmed by treatment of E-MIPs with a SARS-CoV-2 specific monoclonal antibody.

* Corresponding author.
E-mail address: smreddy@uclan.ac.uk (S.M. Reddy).

https://doi.org/10.1016/j.aca.2022.339777

1. Introduction

The coronavirus disease 2019 (COVID-19) pandemic has infected millions of people around the globe [1–5]. The initial symptoms of COVID-19 are similar to other respiratory diseases, but some patients can be asymptomatic [6] or presenting with milder symptoms due to the success of the vaccination programme [7]. Therefore, tracking the causative SARS-CoV-2 is a difficult task. SARS-CoV-2 continues to pose a great health risk to the public with the evolution of more transmissible variants [8]. Whilst current vaccines have reduced the risk of infection, hospitalisation, and mortality, they do not absolutely prevent infection and transmission [8–10]. Therefore, rapid and accurate diagnosis of the virus continues to play a crucial role in the management of the disease enabling a return to near normality in society and in saving lives.

The current gold standard method for SARS-CoV-2 diagnosis is the quantitative reverse transcription polymerase chain reaction (qRT-PCR) test [11–13]. The method detects the presence of viral RNA in nasopharyngeal swab samples with high sensitivity and specificity. However, this assay does have some disadvantages, such as the qRT-PCR requires complex equipment, extensive training for operators, and multiple hours to complete the procedure. These limitations were further accentuated by the rapid growth of the pandemic, as the qRT-PCR did not initially have the screening capacity to keep pace especially at the height of the pandemic [14].

New solutions for COVID-19 detection are in high demand, and one method that has received much traction and also implemented by the National Health Service in the UK is the loop-mediated isothermal amplification (LAMP) method [15,16]. The LAMP method utilises nucleic acid amplification at one temperature, thereby obviating the need for a thermal cycler, essential for conventional PCR. Albeit less quantitative the LAMP method is inherently faster, easier to use, and more cost effective than qRT-PCR assays. While nasopharyngeal and oral swab samples are the accepted mode of sample collection for qRT-PCR [17], the LAMP method uses saliva and/or sputum samples. Saliva is a more attractive medium due to simplicity and no discomfort in collection [18–20], obviating the need for skilled personnel to extract the sample to improve accuracy. Importantly, high viral loads can be present in saliva during the first days of infection, further making it a useful medium to investigate [21,22]. While offering these advantages, there are still disadvantages in the both LAMP and RT-PCR methods affecting accuracy and misdiagnosis or for example cases where individuals have recovered from the infection but are still releasing genetic material from inactivated (non-intact) virus [23]. This can lead to false positive cases skewing case statistics and needlessly taking people out of the workforce.

The other diagnostic assay widely utilised by the public is the SARS-CoV-2 lateral flow test (LFT), which relies on immobilised antibodies to detect nucleoprotein antigen from oral and nasal swabs associated with the virus infection [24]. These tests are easy to use with rapid results, but such immunoassays lack the necessary accuracy to be a reliable SARS-CoV-2 diagnostic test due to its low sensitivity and high false negative/positive rates. For example, the Innova SARS-CoV-2 antigen rapid qualitative LFT offers convenience of use [25–28]. However, data on their efficacy showed that in asymptomatic people, the LFT fails to detect SARS-CoV-2 infection in a substantial proportion. In the Liverpool pilot study, 60% of infected asymptomatic people went undetected, including 33% of those with high viral loads who are at highest risk of infecting others [25]. The LFT can be a useful weapon in the diagnostic arsenal, but when success is restricted only to identifying those who are already symptomatic and/or with a very high viral load, there is clearly a need to improve testing.

Molecularly imprinted polymers (MIPs) are a class of synthetic receptors that can be engineered to selectively recognise biologicals including proteins [29,30] and intact viruses [31,32]. They have antibody-like properties due to their ability to rebind a target antigen of interest. MIPs are easily produced in a one-step chemical reaction for the fraction of the price of antibodies. The target analyte serves as a template molecule around which a functional monomer self-assembles primarily through hydrogen bonding interactions [33]. In the presence of an initiator and crosslinker, a polymer is grown effectively entrapping the target template. Template removal leaves cavities in the MIP and selective rebinding is a function of the target template being recognised by the cavity. Reddy's MIP Group and co-workers have demonstrated the ability of MIPs to selectively capture a model mammalian virus [34]. Subsequent to this research, Parisi et al. [35] demonstrated that nanoparticle-based MIPs were able to inhibit binding of SARS-CoV-2 to its cellular receptor, ACE2. Such examples of virus neutralisation and inhibition open opportunities for MIPs to be used as antiviral agents. MIPs have also been integrated with a range of transducers to produce optical and electrochemical biosensors [36–40]. Recently, electropolymerization has been exploited to produce thin-film MIPs for protein targets on electrode surfaces using redox active functional monomers such as phenols, dopamine, *o*-phenylenediamine and acrylamide [41]. The target template is included in the monomer solution and exposed to the working electrode. Cyclic voltammetry (CV) is used to induce polymerization of the functional monomer at the electrode surface to progressively grow the polymer layer, requiring multiple sequential cycles for optimum film growth. The template, when removed, leaves binding sites selective for the rebinding of target. The subsequent rebinding of target can be investigated also using CV. A small inorganic redox marker such as potassium ferricyanide is used to probe the changing permeability of the MIP depending on whether the target template is bound. In the bound state (when target is present), there is a reduced diffusion of redox marker to the electrode and therefore a small current produced. In the eluted state (when target is absent), the MIP is more permeable to the redox marker resulting in an increase in current. The typical redox marker used is the ferro/ferricyanide redox system. This can be used as a ubiquitous marker for all electrode-based MIPs and obviates the need for the target itself to be electrochemically active. In tandem with cyclic voltammetry, electrochemical impedance spectroscopy (EIS) has been increasingly used to characterise adsorbed biological and polymeric layers on electrode surfaces [42,43]. Supplementary Fig. S1(A) shows the equivalent circuit model for EIS measurement and Fig. S1(B) shows a typical EIS spectrum displaying a characteristic semi-circle and the inflection point in the real impedance signal (Z^{Re}) axis marks the charge transfer resistance (R_{CT}). The R_{CT} (i.e. diameter of the semi-circle) typically increases in the presence of bound layers. There is also typically a corresponding increase in the height of the semi-circle (increase in imaginary impedance, Z^{Im}) with adlayers. Therefore, EIS can be potentially used as a tool to discriminate between different bound and unbound states of, for example, the bare electrode and following MIP integration.

In response to the COVID-19 pandemic, there have been some limited reviews exploring but not limited to the deployment of MIPs to detect SARS-CoV-2. The methodologies are based on identifying either the SARS-CoV-2 nucleoprotein [44] or the full-length spike protein (FL-S) [45,46]. Very recently, this has translated to the first reports of functional MIP-based sensors for SARS-CoV-2. Researchers [47] produced an EIS sensor (within 20 min) using *ortho*-phenylenediamine (oPD) monomer-based MIP to imprint the receptor binding domain (RBD) component. They calculated a theoretical viral load equivalence sensitivity of

3–4.8 × 10^2 copies/μL (i.e. 3 - 4.8 × 10^5 copies/mL). A second group [48] have reported detection of FL-S from nasopharyngeal swabs using electropolymerized 3-aminophenylboronic acid (APBA) MIPs. Analyte measurement was possible within 15 min and a limit of detection (LOD) of 64 fM was reported using differential pulse voltammetry. While the APBA serves to attach to *cis*-diols of glycoproteins such as the FL-S, it should be noted that APBA is not selective to any one glycoprotein and therefore will be prone to interference from other glycoproteins.

It should be noted that the spike protein is prone to multiple mutations as the virus evolves, which could limit the application of this approach. A holistic virus imprinting approach, taking into consideration the template's full characteristics (size, shape and presentation of spike) offers the potential for MIP-based diagnostic to evolve with the virus. To this end, we have found that imprinting of the SARS-CoV-2 virion particle (whole intact virus) as a template has been largely overlooked with only one publication [49] at the time of writing this paper. In their work, a graphene-based electrode was integrated with an E-MIP based on pyrrole as functional monomer in conjunction with 3-aminophenylboronic acid (APBA) to imprint whole virus, in a sensor production process taking 1 h. All rebinding studies were performed in control solutions only and did not use real samples. As mentioned earlier an approach using APBA is prone to interference due to the presence of interfering glycoproteins.

In our approach, we use an acrylamide-based hydrogel MIP to electrochemically imprint the whole intact virus in a MIP production process taking 2–5 min and we demonstrate the measurement of SARS-CoV-2 whole virus in actual biological samples (saliva) within 5 min. Specifically, we evaluate and present proof-of-concept findings that electrochemically grown MIPs (E-MIPs) imprinted with SARS-CoV-2 pseudoparticles (replication incompetent lentiviruses embedded with the SARS-CoV-2 spike protein [50]) can be used to selectively recognise the template particles. This is achieved by the MIP identifying with the virion shape and/or the presence of the spike protein. Subsequently, E-MIPs are prepared for virus capture from saliva and analysis. The E-MIPs are interrogated electrochemically (using CV and EIS) with a view to be used by untrained and trained personnel alike (see Fig. 1). We present an evaluation of an evolving (MIP) technology and demonstration of proof of concept. We explain the simplicity of the method to determine SARS-CoV-2 in untreated saliva samples, which in itself is an indication of how it can easily replace the laboratory-based LAMP method, with minimal labour and skill required.

2. Experimental section

2.1. Materials

N-hydroxymethylacrylamide (NHMA, 48% w/v), *N,N′*-methylenebisacrylamide (MBAm), phosphate buffered saline tablets (PBS, 10 mM, pH 7.4 ± 0.2), potassium ferricyanide ($K_3[Fe(CN)_6]$), potassium chloride (KCl), sodium nitrate ($NaNO_3$), potassium peroxydisulfate (KPS) and artificial saliva (SAE0149, pH 6.8) were supplied from Sigma, Merck. Buffers were prepared in ultra-pure water (UPW, 18.2 ± 0.2 MΩ cm) and filter sterilised (0.22 μm). Inactivated influenza A virus subtype H9N2 (IAV/H9N2, 9.0 $\log_{10}$ pfu/mL) was kindly donated by Prof. Munir Iqbal (The Pirbright Institute, UK). Inactivated, purified porcine reproductive and respiratory syndrome virus 1 (PRRSV) was prepared as described previously [34].

2.2. Methods

Production of SARS-CoV-2 pseudoparticles and recombinant human monoclonal antibody CR3022.

SARS-CoV-2 pseudoparticles (pps) were prepared as previously described [50]. For a simplified schematic of the protocol, the reader is also referred to Ref. [51]. In brief, HEK293T cells are transfected with 0.6 μg of both p8.91 (HIV-1 gag-pol) and pCSFLW (lentivirus backbone expressing a firefly luciferase reporter gene) and 0.5 μg pCDNA3.1 SARS-CoV-2 spike D614 in OptiMEM with 10 μL polyethyleneimine 1 μg/mL (Sigma). The viral supernatant was harvested at 48 and 72 h post-transfection, centrifuged to remove cell debris and stored at −80 °C. SARS-CoV-2 pps were concentrated by ultracentrifugation and were pelleted through a sterile 20% sucrose cushion at 23,000 rpm for 2 h at 4 °C using a SW32 rotor and XPN-100 Ultracentrifuge (Beckman Coulter). Virus pellets were gently reconstituted in 600 μL of PBS. SARS-CoV-2 pps were inactivated by incubation with 0.1% β-propiolactone (BPL; Sigma) at 4 °C whilst rolling. Following this, incubated at 37 °C for 2 h to hydrolyse BPL. SARS-CoV-2 pps were titrated before and after BPL inactivation by titration on HEK293T cells, previously transfected with 500 ng of a human ACE2 expression plasmid (Addgene, Cambridge, MA, USA). Following incubation at 37 °C, 5% CO_2 for 72 h. Firefly luciferase activity was then measured with BrightGlo luciferase reagent and a GloMax-Multi + Detection System (Promega, Southampton, UK) to determine infected wells and allow calculation of the median 50% tissue culture infective does ($TCID_{50}$). Virus titres were converted from $TCID_{50}$/mL to pfu/mL using a multiplication factor of 0.7. Vectors for expression of SARS-CoV and SARS-CoV-2 spike specific human monoclonal antibody (mAb) CR3022 [52] was kindly provided by Prof. Ray Owens, Protein Production UK (PPUK), Rosalind Franklin Institute, UK. Recombinant mAb CR3022 was expressed by transient co-transfection of Expi293F™ cells (Gibco™ A14527, Thermo Fisher Scientific) with plasmids coding for the IgG1 heavy chain and kappa light chain [53], using Polyethylenimine (PEI) MAX® (molecular weight 40 kDa, Polysciences 24765). Following 3 days incubation at 37 °C, the cell culture supernatant was harvested, and IgG purified by Protein G chromatography (Cytiva 17040501). The pH neutralised eluate was dialysed in PBS and the purified mAb CR3022 concentration was determined by A280/1.4 to be 1.8 mg/mL.

2.3. E-MIP production

Thin-film hydrogel layers were fabricated directly onto screen-printed electrodes (SPEs, (Au-BT), Metrohm) by electrochemical polymerization using cyclic voltammetry (CV). A 50 μL PBS or PBS diluted synthetic saliva solution containing SARS-CoV-2 pps (3.0–5.6 $\log_{10}$ pfu/mL), 1.33 M NHMA as the functional monomer, 41.5 mM MBAm as the cross-linker, 0.29 M $NaNO_3$, and 48.15 mM KPS was deposited onto the SPE. The potential was then cycled between −0.2 V and −1.4 V for 5–25 cycles at 50–100 mV s^{-1} (4–10 min, RT, 22 ± 2 °C). To remove template virus, elution was also carried out electrochemically at −0.5 V and 1.5 V for 5 cycles at 175 mV s^{-1} (~5 min, RT, 22 ± 2 °C) using PBS (50 μL). Non-imprinted polymer controls (E-NIPs) were produced in a similar manner, but in the absence of virus template, and eluted for consistency.

2.4. Electrochemical characterisation of E-MIP

Polymer deposition was tracked via typical CV scans (triplicate) of an external 5 mM potassium ferricyanide solution containing 0.5 M KCl as supporting electrolyte (50 mV s^{-1}). Electrochemical impedance spectroscopy (EIS) measurements were conducted using the same redox couple, at a standard potential of 0.1 V (±0.01 V) with 10 scans of frequencies, and a sinusoidal potential peak-to-peak with amplitude 0.01 V in the 1–100000 Hz frequency range. An equivalent circuit was fitted for all EIS experiments using the FRA32 module (Randles Circuit) - composed of a charge transfer

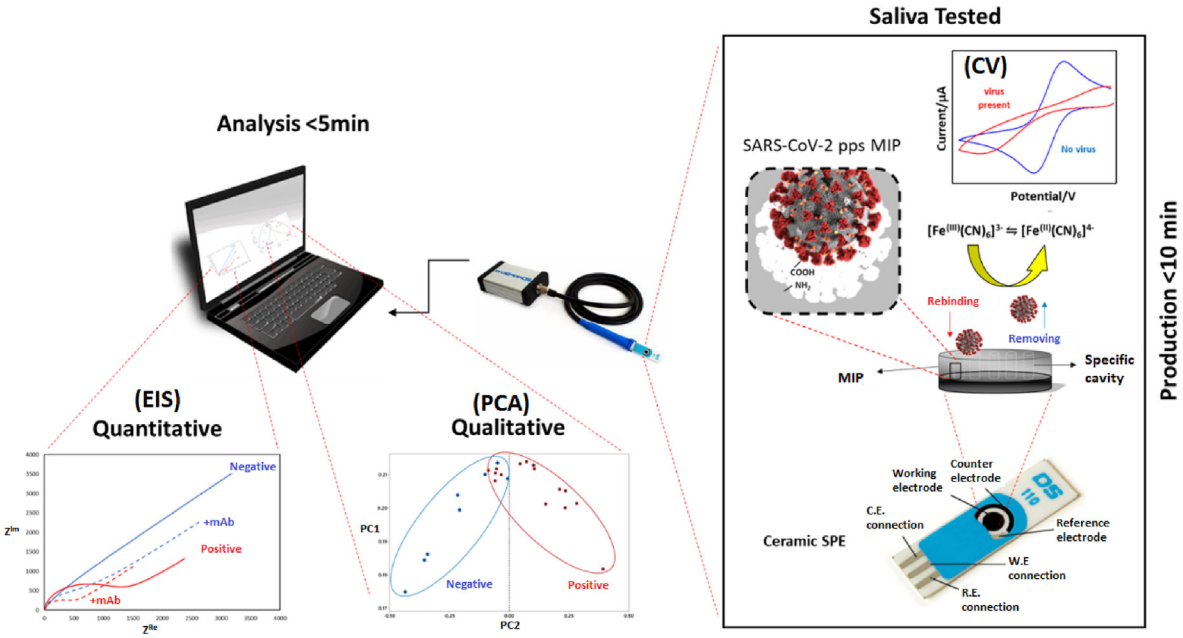

Fig. 1. Schematic illustration of the proof-of-concept components, detection principle and detection procedure of COVID-19 E-MIPs. Initially, the SARS-CoV-2 pseudoparticle (pps) imprinted MIP is electrodeposited onto a disposable screen-printed electrode (SPE). In the presence of SARS-CoV-2 pps the anodic/cathodic peak currents to an external redox marker (ferricyanide) decrease and EIS spectra show a corresponding change, leading to qualitative and quantitative approaches to *in-situ* SARS-CoV-2 detection.

resistance between the solution and the electrode surface (R_{CT}), solution resistance (R_S), the Warburg impedance (Z_W, associated with the diffusion of the electroactive species from the solution towards the electrode surface), and the double layer capacitance (C_{dl}), (Supplementary Fig. S1). All electrochemical measurements were performed using a Metrohm Autolab PGSTAT204 and NOVA2.1.4 software. Template rebinding studies were performed by exposing E-MIP modified SPEs to 50 μL of target SARS-CoV-2 pps (in the range 3—5.6 $\log_{10}$ pfu/mL) for a period of 2 min. Subsequent to template rebinding, 50 μL of mAb CR3022 (6.2 μM) were also applied to the SPE chip for 2 min at RT 22 ± 2 °C (0.9 mg/mL). After each template rebind and mAb CR3022 treatment, the SPE chip was electrochemically interrogated in the presence of ferricyanide redox marker (5 mM) using cyclic voltammetry and EIS.

2.5. PCA for qualitative determination of SARS-CoV-2

Statistical analysis utilising principal component analysis (PCA) was conducted through Minitab, Version 20.3. Plots were carried out using the first 5 voltammetric current density scan values without any previous pre-processing and scaling from the modified SPE process as input.

2.6. Proof of concept study with human saliva samples

Patient saliva samples were kindly provided by the NHS COVID-19 LAMP Saliva Testing Laboratory (Preston, UK). Samples were processed in line with the Lancashire & South Cumbria COVID-19 LAMP Saliva Testing Programme for testing staff. Initial laboratory confirmation for SARS-CoV-2 on these specimens was done using the LAMP method. Anonymised patients were asked to produce a clear and non-viscous saliva sample (not containing phlegm or sputum) 10 min before oral hygiene being carried out, drinking, smoking, or eating. Lysis buffer (Rapilyze) was added to the saliva specimen to expose virus genetic content prior to LAMP analysis. An aliquot (0.5 mL) of each sample (prior to adding lysis buffer) was set aside for E-MIP analysis. Negative samples were stored at 4 °C on a daily-basis; positive samples were stored at −80 °C and thawed at room temperature prior to E-MIP analysis.

To assess our E-MIP-SPE method using the patient samples, 15 SARS-CoV-2 LAMP positive and 9 LAMP negative saliva samples were used in the production of polymer-modified SPE surfaces by spiking the monomer solution with 50 μL of the saliva sample, followed by CV (See *E-MIP production*). The E-MIP and E-NIP SPEs thus produced were washed with PBS to remove any non-specifically bound material and then characterised using CV and EIS. The E-MIP and E-NIP entrapped saliva samples were further investigated by exposing the modified SPEs to 50 μL of SARS-CoV-2 mAb CR3022 for 2 min (0.9 mg/mL). Again, samples were analysed using CV and EIS.

3. Results and discussion

3.1. Electrochemical characterization of E-MIP

Fig. 2A and B shows the polymerization cycles for E-MIP (SARS-CoV-2 pps 5.6 $\log_{10}$ pfu/mL) and E-NIP respectively. As expected, the peak cathodic current at −1.0 to −1.2 V decreased with each cycle due to the free-radical initiated electropolymerization of acrylamide monomer and subsequent deposition of poly-acrylamide on the electrode surface [41,54,55]. In order to elute the template, we first investigated using the well-established sodium dodecyl sulphate/acetic acid (SDS/AcOH; 10% v/v) eluent to extract biologicals from MIPs [56,57], but discovered that these conditions were stripping away the electropolymerized E-MIP (the peak currents for the redox label returned to bare electrode levels). Due to the potential harsh nature of using these conventional MIP elution conditions, we investigated cycling the voltage at more positive potentials (+1.5 V vs Ag/AgCl reference) post-polymerization in PBS to remove the template (Supplementary Fig. S2). This was found to effectively remove the template without apparently compromising the integrity of the pre-formed E-MIP.

Ferricyanide was used as a redox label to confirm that E-MIP or E-NIP was deposited on the bare electrode. A reduction in peak

current to the redox marker was a firm indicator that a polymer layer was formed on the electrode surface. Fig. 2C shows the ferro-ferricyanide cyclic voltammograms comparing the bare electrode and following MIP formation, template elution and template rebinding. Fig. 2D shows the corresponding cyclic voltammograms for the E-NIP control polymer. The E-MIP follows the expected pattern in change in peak currents. There is a significant decrease in current upon MIP formation, compared with the bare electrode (SPE). Upon template elution, the redox peak increases to an intermediate stage but still lower than the bare electrode, confirming that template has been removed (allowing more redox marker to diffuse to the electrode). Upon template rebinding, the current decreases due to a decrease in permeability of the redox marker to the electrode. The E-NIP also behaves as expected. Since there is no template to remove, it also confirms that electrochemical elution conditions do not affect the integrity of the polymer adlayer. Indeed, the NIP layer is more uniform and homogenously produced compared with the MIP. The presence of the virus serves to impede the otherwise natural course of monomer polymerization and crosslinker incorporation. The polymerization process therefore needs to navigate around the template and entraps it between the growing polymer chains during the process resulting in a more porous polymer layer structure on the electrode. Polymer growth in the NIP, by contrast, is less tortuous due to the absence of template, allowing it to form a more rigidly coupled, homogeneous and dense layer with inherently low porosity. Therefore, for an equivalent

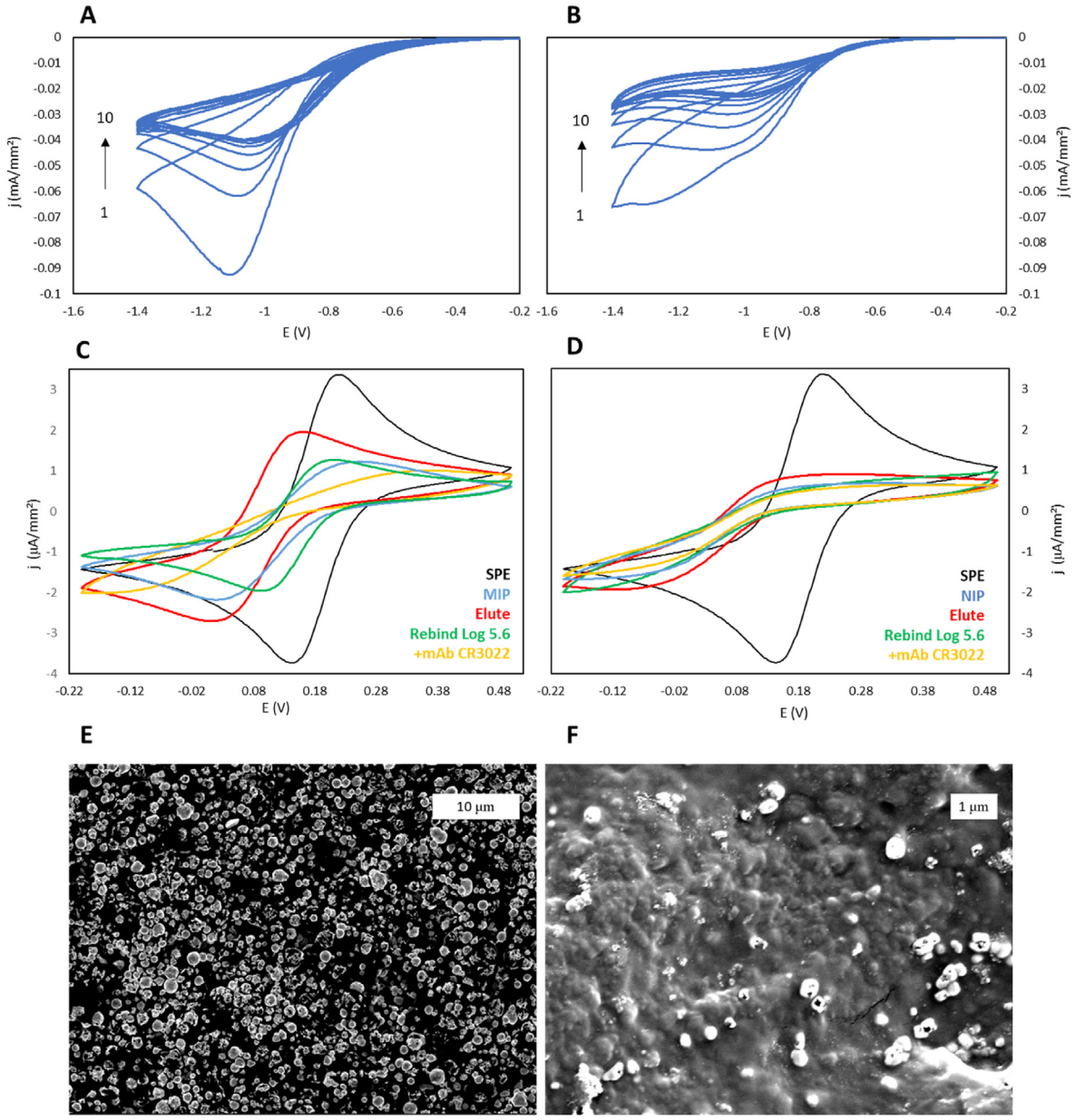

Fig. 2. Typical CVs illustrating the current density (j) changes in a 10 scan electropolymerization process (~5 min, RT, 22 ± 2 °C) of SARS-CoV-2 pps (5.6 $\log_{10}$ pfu/mL) imprinted MIP (A) and NIP (B) layers in synthetic saliva at a scan rate of 50 mV s^{-1}. CV characterisations (3rd scan) using 5 mM potassium ferricyanide solution containing 0.5 M KCl at a scan rate of 50 mV s^{-1} of: MIP (C) and NIP (D) layers before (SPE) and after polymer modifications and following elution, pps rebinding and mAb addition. Rebinding (2 min, RT 22 ± 2 °C) conducted using 50 µL of 5.6 $\log_{10}$ pfu/mL SARS-CoV-2 pps and then subjected to 50 µL mAb CR3022 (2 min, RT 22 ± 2 °C, 0.9 mg/mL). SPE represents the bare (unmodified) electrode. SEM scans of SPE before (E) and after polymerization (F) demonstrating the presence of polymer modification and topography change. Scans were conducted using a Thermo Fisher Quattro S scanning electron microscope at 5 kV and SPEs were measured in triplicate using 3 different sites.

number of polymerization cycles, the NIP will incorporate more monomer and crosslinker than the MIP. Fig. 2D and E represent scanning electron micrographs of the bare gold electrode and E-MIP coated electrode respectively.

3.2. SARS-CoV-2 pseudoparticle detection using E-MIPs

Cyclic voltammograms for SARS-CoV-2 pps template rebinding at a high viral titre (5.6 $\log_{10}$ pfu/mL) are shown in Fig. 2C and D. The decrease in peak current did not correlate with increasing viral titre (data not shown), and so at best, it presents a qualitative (yes/no) approach to determining the presence of virus. We were able to detect the presence of template in the range 4.1–6.0 $\log_{10}$ pfu/mL. This is an acceptable range for the determination of SARS-CoV-2 in saliva levels found using genome copy analysis [58] and the lower limit (calculated based on 3σ/slope) is comparable to the LOD (4.0 $\log_{10}$ pfu/mL) reported by Hashemi et al. in their graphene electrode-based MIP system for measuring SARS-CoV-2 whole virus [49]. Based on the virus particle concentration in their control experiments, they also calculated that this equated to a LOD of 11.3 fg/mL. By extrapolation, this suggests our method has a LOD of 88.0 fg/mL. It is of note that real samples were not tested in their study.

PCA and factor analysis was used to discriminate and semi-quantitate between the presence and absence of SARS-CoV-2 pps in MIP and NIP formation. Fig. 3 shows a clear discrimination between NIP control (no SARS-CoV-2 pps present) and MIP loaded with SARS-CoV-2 pps, with 99.5% of the of the variance explained by principal components 1 and 2. The factor analysis (Fig. 3A) illustrates the concentration dependency as the variable factor in the component separation. Each of the four quadrants in the PCA biplot hold concentrations of SARS-CoV-2 pps in the form of high, mid, low, and negative as a consequence (Fig. 3B). This allows for the discrimination between the viral loading samples and suggests the possibility of determining any artifacts or template virions within the polymer synthesis and deposition at the working electrode.

In addition to cyclic voltammetry, EIS was used to further investigate the rebinding of SARS-CoV-2 pps to MIP and NIP. Fig. 4A compares the Nyquist plots for bare electrode, MIP and NIP. The bare gold SPE (black line) was characterised by a small impedance ($\approx$ 500 Ω) a resistance to charge transfer (R_{CT}) of 1800 ± 100 Ω, the latter indicating the expected small resistance toward redox conversion and a high electron transfer on the bare electrode surface. It should be noted that the R_{CT} in the EIS spectrum (but not the form of the spectrum) for the bare SPE can vary between electrodes due to batch-to-batch variation in printed electrode material. Subsequent changes to R_{CT}, real (Z^{Re}) and imaginary (Z^{Im}) impedances, will be relative to the baseline EIS response of the SPE used. Both MIP and NIP modified electrodes showed an increase in impedance ($Z^{Re} \approx 3000$ Ω) and an increase in R_{CT} to 7000 Ω, demonstrating an increased resistance to redox conversion. This would be expected since both MIP and NIP presented a barrier to diffusion of the ferricyanide redox marker. We subsequently treated MIP and NIP layers with a SARS-CoV-2 specific mAb CR3022. MIP samples elicited a significant change in impedance likely due to antibody binding to entrapped SARS-CoV-2 pps ($Z^{Re} \approx 5000$ Ω) and an associated $R_{CT} \approx 10000 \pm 1000$ Ω demonstrating high resistance to redox conversion. Conversely, the NIP showed only a small increase in impedance upon mAb CR3022 treatment (from 3000 to 3400 Ω) with no significant change in R_{CT}. This is possibly attributed to some non-specific binding of antibody to the NIP.

We investigated a range of SARS-CoV-2 pps loadings on the MIPs (Fig. 4C) which demonstrated that all viral loadings (1.0–6.0 $\log_{10}$ pfu/mL) were grouped together with R_{CT} values at or below 2000 Ω. However, with the eluted MIP (virus removed) or below 2.0 $\log_{10}$ pfu/mL viral load on the MIP, the corresponding Nyquist plot resembled that of NIP (zero virus) allowing us to determine a threshold of 2.0 $\log_{10}$ pfu/mL below which the E-MIP sensor could not determine SARS-CoV-2. The clear separation in impedance characteristics between presence and absence of virus on MIP suggests that this method could be used qualitatively to discriminate between positive and negative COVID-19 cases, essentially with no requirement for post measurement data processing through principal component analysis. This radically speeds up the time to a result to less than 5 min.

By extracting the charge transfer resistance values, we were able to produce a calibration plot for the semi-quantitative determination of SARS-CoV-2 pps in the range 3.0–7.0 $\log_{10}$ pfu/mL with a limit of detection of 4.9 $\log_{10}$ pfu/mL (Fig. 4D). Whereas there was a linear correlation between viral load and R_{CT} at medium to high viral loadings of 4.0–7.0 $\log_{10}$ pfu/mL, the R_{CT} responses in the range 2.0–4.0 $\log_{10}$ pfu/mL did not differ significantly. Nonetheless, we present a wide linear range and whereas it may not cover 8 logs as with the PCR method, it should be noted that we present a method to detect SARS-CoV-2 in untreated saliva with no amplification of virus material. Our E-MIPs also showed selectivity for template SARS-CoV-2 pps, with an imprinting factor of 3:1, and specificity (significance = 0.06) when cross-reacted with similar concentrations of either porcine reproductive and respiratory syndrome virus 1 (PRRSV) or influenza A virus subtype H9N2 (IAV) (Supplementary Fig. S3).

3.3. SARS-CoV-2 detection in clinical saliva samples

The richness in information from the whole Nyquist plot and the high discrimination in overall signal for the different E-MIP viral loading conditions (Fig. 4A and C) offers a route to a plausible rapid and sensitive system for SARS-CoV-2 determination. We investigated this further by testing 24 patient saliva samples, which had been previously tested for SARS-CoV-2 using the LAMP method. Only a small saliva sample (50 μL) was required with no dilution or pre-treatment. PCA biplots for polymer formation using the 'qualitative' approach were again determined (Fig. 5A), demonstrating two clusters for each of the positive and negative samples, showing 66.6% agreement with LAMP positive results and 88.9% agreement with LAMP negative results. Interestingly, our study revealed that a degree of overlap was present in the discrimination method, with five samples from the LAMP positive results presenting as negative results using our E-MIP approach. Overall, there was 75% agreement between our E-MIP method and the LAMP method.

There is a difference in the EIS response when switching from imprinting of control pps in PBS or saliva (Fig. 4A and C) to imprinting of virus within a real saliva sample (Fig. 5B). The latter shows that the E-MIP device returns small Z^{Re} and Z^{Im} values when the virus is entrapped in the MIP production process indicating a positive test result. The negative test results possess significantly higher Z^{Re} and Z^{Im} values to those of either the NIP (no virus) or the eluted MIP from Fig. 4A. As a confirmatory measure of entrapped SARS-CoV-2 in positive samples, all representative samples were treated with SARS-CoV-2 S-specific mAb CR3022 (Fig. 5B, green and grey lines). Only COVID-19 positive samples elicited a significant change in the Nyquist plots due to antibody binding to entrapped virus presenting with the spike protein. Interestingly, COVID-19 negative samples also showed a small change in Z^{Re} and Z^{Im} upon antibody treatment, possibly due to non-specific binding of antibody. Surprisingly though, the direction of changes in impedance observed for the positive cases upon mAb CR3022 treatment was unexpected. Whereas we expected an increase in impedance due to specific adsorption and layering of antibodies to the MIP-surface-entrapped virus, there was instead a decrease in both Z^{Re} and Z^{Im}

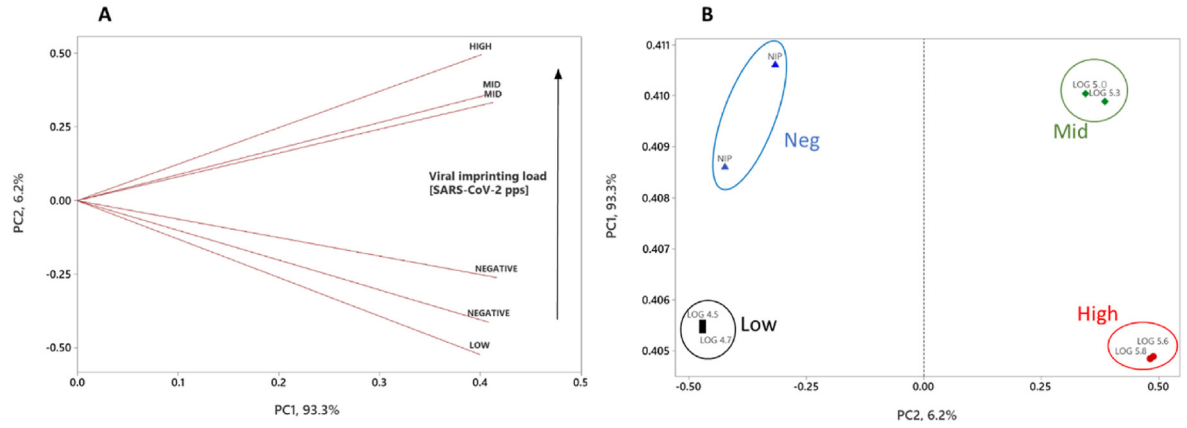

Fig. 3. Factor analysis (A) and PCA (B) for polymer formation and SARS-CoV-2 pps capture (~5 min, RT, 22 ± 2 °C) in the 'qualitative' approach. Each data point represents triplicate inputs collected from CV data using the current change in the first 5 cycles as variables. Groupings illustrate SARS-CoV-2 pps titres imprinted using saliva, based on $\log_{10}$ pfu/mL: Neg = 0; Low = 4.5–4.7; Mid = 5.0–5.3; High = 5.5–5.6.

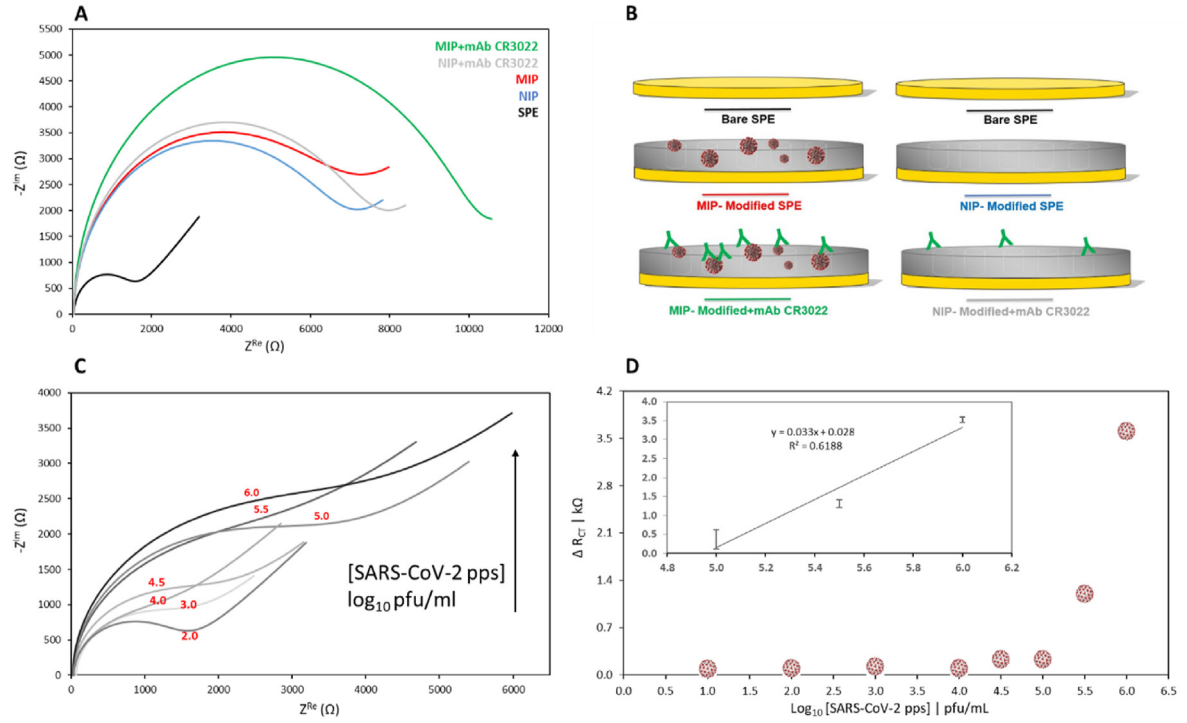

Fig. 4. (A) Nyquist plots for SPEs comparing the E-MIP and E-NIP layers, following SARS-CoV-2 pps rebinding and coupling with SARS-CoV-2 mAb CR3022; data fitted with Randles equivalent circuit, data represents mean, n = 3. (B) Schematic representation of the SPE modification stages corresponding to responses seen in Nyquist plots in Fig. 4A. (C) Nyquist plots for SARS-CoV-2 pps rebinding; data fitted with Randles equivalent circuit, data represents mean, n = 3. (D) Calibration curve for SARS-CoV-2 pps rebinding (2min, RT 22 ± 2 °C) using R_{CT} data as input, insert shows LDR following axis titles, data represents mean ± SD, n = 3.

as well as in the associated R_{CT} suggesting a decreased resistance to (increased diffusion of) the ferro/ferricyanide redox marker electrode process. It is noteworthy that this unexpected decrease occurred consistently only with the positive cases. We speculate that the antibody binding with SARS-CoV-2 antigen is leading to the antibody-antigen complex stripping away from the electrode into the surrounding solution, and hence the decrease in Z^{Re} and Z^{Im}. The binding affinities of acrylamide-based MIPs for proteins are typically in the sub-micromolar range [59]. Given that the affinity of CR3022 for the RBD is very high at 0.125 nM [52], such a stripping mechanism by the antibody is plausible. Voltammograms (Fig. 5C) for representative positive and negative samples confirm that the peak anodic current of the ferro/ferricyanide CV show increased values for the MIP positive samples following antibody addition, confirming that the E-MIP polymer layer is becoming more permeable to the redox marker. Conversely, the negative (NIP-like) samples retain their low CV response to the redox marker following antibody addition. That the E-MIP increases its permeability is not surprising if we consider the possible modes of action of the antibody. More than one antibody can bind to the presenting virus surface in the E-MIP layer. These antibodies can then agglomerate causing the entrapped virus to decouple from the E-MIP on the electrode surface.

Table 1 gives a comparison of performance of our MIP-based SARS-CoV-2 electrochemical sensor with others published at the time of writing this paper. While the template can vary from whole

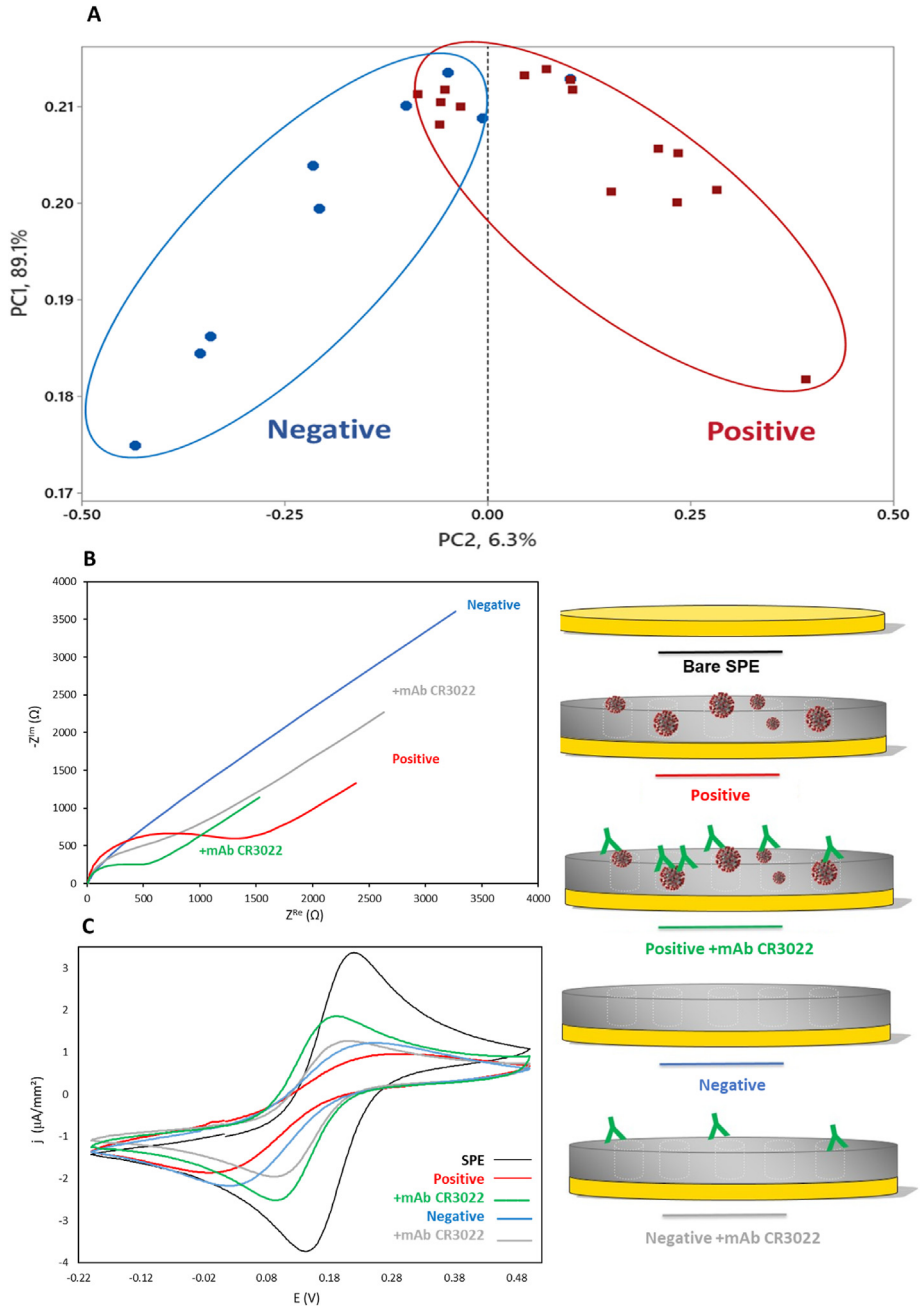

Fig. 5. (A) PCA for polymer formation using 'qualitative' approach on 24 LAMP confirmed COVID-19 positive (red) and negative (blue) human saliva samples. (B) Typical Nyquist plots for SPEs comparing positive (MIP) and negative (NIP) confirmed saliva samples before and after treatment with 50 μL mAb CR3022 (0.9 mg/mL, 2 min, RT, 22 ± 2 °C). Fitted with Randles equivalent Circuit, data represents mean, n = 10. (C) Typical CV characterisations (3rd scan) of representative positive (MIP) and negative (NIP) sample depositions before and after 50 μL antibody treatment (0.9 mg/mL, 2 min, RT, 22 ± 2 °C). Schematic representations of each stage of treatment of positive and negative samples given on the right-hand side.

virus, nucleoprotein, FL-S to RBD, it can be seen our method to determine the whole virus compares favourably with [49], with the advantage that we have been able to make determinations in actual COVID-19 positive and negative saliva samples. Indeed, it is remarkable that besides our work, to date, there is only one paper [44] which tests for SARS-CoV-2 using real patient samples. It should be noted that our calculated LOD (88.0 fg/mL) is approximately one order of magnitude higher than Hashemi et al. (11.3 fg/mL). This could be related to the difference in monomer/electrode systems used in the two studies. Their use of a graphene nano-electrode based system could enhance the signal-to-noise ratio resulting in a higher observed MIP sensitivity with lower LOD.

4. Conclusions

We present a simple MIP-based electrochemical method for detecting SARS-CoV-2 requiring only 50 μL of an untreated saliva sample. Our technique relies on the electrochemical molecular imprinting process to entrap the virus onto a low-cost disposable screen-printed electrode surface. MIP production time is less than 5 min. Subsequent electrochemical impedance spectroscopy (<2 min) produces a Nyquist plot which can discriminate between positive and negative cases. Time to result is therefore less than 10 min even when considering a washing stage (30s). The overall Nyquist plot serves as a potential discriminator between COVID-19

Table 1
Comparison of the analytical performance of our method against recently published electrochemical MIP sensors for SARS-CoV-2 using various imprinted templates. p(d): production (and detection, based on MIP rebinding); pps: pseudoparticles (replication incompetent lentiviruses embedded with the SARS-CoV-2 spike protein); LOD: limit of detection; LDR: linear dynamic range. * evaluated using pfu/mL to fg/mL relationship derived in Ref. [49] for fair comparison with our method.

MIP Sensor [Ref]	Template	Time p(d)	LDR	LOD
polyNHMA/Au-SPE (**Our method**)	Whole virus (pps)	<10 min (2 min) tested on **COVID-19 positive and negative** saliva	Log_{10} 4.0 −6.0 pfu/mL	*88.0 fg/mL (Log_{10} 4.9 pfu/mL)
polypyrrole-boronic acid/Graphene-GCE [49]	Whole virus	>1 h (1 min) tested on spiked PBS only	0.7−9.0 fg/mL	11.3 fg/mL (Log_{10} 4 pfu/mL)
Poly-*m*-phenylenediamine/Au-SPE [44]	Nucleoprotein (51 kDa)	>1 h (15 min) tested on **COVID-19 positive** nasopharyngeal swab	Up to 5.7 pg/mL	0.7 ng/mL (15 fM)
ortho-phenylenediamine/Au-SPE [47]	RBD (35 kDa)	>15 min (20 min) tested on spiked PBS/saliva only	2.0−40.0 pg/mL	0.7 pg/mL (20 fM)
3-aminophenylboronic acid (APBA)/Au-TFME [48]	Spike protein (ncovS1, 45 kDa)	>1 h (15 min) tested on spiked COVID-19 negative nasopharyngeal swab only	1.1−4.8 pg/mL	4.8 pg/mL (64 fM)

positive and negative samples exhibiting a clear separation in real and complex impedances between the two cases. Whereas our electrochemical device demonstrated an overall 75% agreement with the LAMP method, significantly, our method produced a negative result in a third of the LAMP positive cases. This requires further investigation using a larger patient sample size. Additionally, any further validation of our E-MIP method will require a comparison to the gold standard RT-PCR method. Compared with the LAMP method, our E-MIP method does not require manipulation of the virus to release proteins and/or RNA nor subsequent amplification of genetic material. It relies on a low-cost electrochemically grown polymer that captures the whole intact virus from saliva. Pre-treatment of the sample is not required, which saves significant time. We show that subsequent mAb CR3022 treatment of the MIP-entrapped virus can be used for further confirmation of COVID-19 positive cases, and it may be useful to discriminate between SARS-CoV-2 and other respiratory viruses.

CRediT authorship contribution statement

H.F. EL Sharif: contributed to conception and design of the study, performed the study and analysis, wrote the manuscript. **S.R. Dennison:** contributed to conception and design of the study. **M. Tully:** produced and characterised the mAb CR3022 monoclonal antibody and SARS-CoV-2 pseudoparticles. **S. Crossley:** produced and characterised the mAb CR3022 monoclonal antibody and SARS-CoV-2 pseudoparticles. **W. Mwangi:** produced and characterised the mAb CR3022 monoclonal antibody and SARS-CoV-2 pseudoparticles. **D. Bailey:** produced and characterised the mAb CR3022 monoclonal antibody and SARS-CoV-2 pseudoparticles. All authors contributed to manuscript revision, read, and approved the submitted version. **S.P. Graham:** contributed to conception and design of the study. **S.M. Reddy:** contributed to conception and design of the study, wrote the manuscript.

Declaration of competing interest

The authors declare that they have no known competing financial interests or personal relationships that could have appeared to influence the work reported in this paper.

Acknowledgments

The authors are grateful to the Royal Society of Chemistry COVID-19 Action fund (H20-188), the Daiwa Anglo-Japanese Foundation (13094/13916), the Faculty of Science and Technology at the University of Central Lancashire (UCLan), and UKRI Biotechnology and Biological Sciences Research Council (BBSRC) Institute Strategic Programme and Core Capability Grants to The Pirbright Institute (BBS/E/I/00007031, BBS/E/I/00007034, and BBS/E/I/00007039) and BBS/E/I/COV07001 for providing funds to support this work. The authors also wish to thank Philip Houldsworth, Paul Regan and Prof. Anthony Rowbottom from the NHS COVID-19 LAMP Saliva Testing Laboratory (Preston, UK), part of the Lancashire & South Cumbria COVID-19 LAMP Saliva Testing Programme for supplying clinical saliva samples. We thank Prof. Ray Owens, PPUK, Rosalind Franklin Institute, for providing the vectors for expression of mAb CR3022, Prof. Munir Iqbal, The Pirbright Institute, for providing inactivated influenza A virus, and Dr James Kelly and Ahmed Mohamed for assistance with SARS-CoV-2 propagation and purification.

Appendix A. Supplementary data

Supplementary data to this article can be found online at https://doi.org/10.1016/j.aca.2022.339777.

References

[1] A.N. Devi, Overview of COVID-19 pandemic: transmission, epidemiology and diagnosis, Journal of Pharmaceutical Research International 33 (2021) 174−181.
[2] P. Dey, S. Vaijayanthimala, V.S. Dalvi, A. Jain, D. Gola, M. Bajpai, R.K. Bharti, N. Chauhan, COVID-19: understanding the pandemic emergence, impact and infection prevalence worldwide, J. Pure Appl. Microbiol. 14 (2020) 2235−2251.
[3] A. Kumar, R. Singh, J. Kaur, S. Pandey, V. Sharma, L. Thakur, S. Sati, S. Mani, S. Asthana, T.K. Sharma, S. Chaudhuri, S. Bhattacharyya, N. Kumar, Wuhan to world: the COVID-19 pandemic, Front. Cell. Infect. Microbiol. 11 (2021).
[4] S.I. Mallah, O.K. Ghorab, S. Al-Salmi, O.S. Abdellatif, T. Tharmaratnam, M.A. Iskandar, J.A.N. Sefen, P. Sidhu, B. Atallah, R. El-Lababidi, M. Al-Qahtani, COVID-19: breaking down a global health crisis, Ann. Clin. Microbiol. Antimicrob. 20 (2021).
[5] M.H. Peng, Outbreak of COVID-19: an emerging global pandemic threat, Biomed. Pharmacother. 129 (2020).
[6] A. Tiotiu, H. Chong Neto, A. Bikov, K. Kowal, P. Steiropoulos, M. Labor, I. Cherrez-Ojeda, H. Badellino, A. Emelyanov, R. Garcia, G. Guidos, Impact of the COVID-19 pandemic on the management of chronic noninfectious respiratory diseases, Expet Rev. Respir. Med. 15 (2021) 1035−1048.
[7] Q. Li, X.M. Zhan, J. Wang, H.Z. Lu, Considerations and guidance to control the rebound in COVID-19 cases, Biosci. Trends. 15 (2021) 341−344.
[8] P. Sah, T.N. Vilches, S.M. Moghadas, M.C. Fitzpatrick, B.H. Singer, P.J. Hotez, A.P. Galvani, Accelerated vaccine rollout is imperative to mitigate highly transmissible COVID-19 variants, Eclinicalmedicine 35 (2021).
[9] N.G. Davies, C.I. Jarvis, W.J. Edmunds, N.P. Jewell, K. Diaz-Ordaz, R.H. Keogh, C.C.-W. Grp, Increased mortality in community-tested cases of SARS-CoV-2 lineage B.1.1.7, Nature 593 (2021) 270. -+.
[10] T. Farinholt, H. Doddapaneni, X. Qin, V. Menon, Q.C. Meng, G. Metcalf, H. Chao, M.C. Gingras, V. Ayadhanula, P. Farinholt, C. Agrawal, D.M. Muzny, P.A. Piedra, R.A. Gibbs, J. Petrosino, Transmission event of SARS-CoV-2 delta variant reveals multiple vaccine breakthrough infections, BMC Med. 19 (2021).
[11] J. Gao, L. Quan, Current Status of Diagnostic Testing for SARS-CoV-2 Infection and Future Developments: A Review, vol. 26, Medical Science Monitor, 2020.
[12] N. Gupta, S. Augustine, T. Narayan, A. O'Riordan, A. Das, D. Kumar, J.H.T. Luong, B.D. Malhotra, Point-of-Care PCR Assays for COVID-19 Detection, vol. 11, Biosensors-Basel, 2021.
[13] N. Joyce, L. Seim, M. Smerina, The dynamics of SARS-CoV-2 (RT-PCR) testing, Case Report Med. (2021) 2021.
[14] Y. Zhou, L. Zhang, Y.-H. Xie, J. Wu, Advancements in Detection of SARS-CoV-2 Infection for Confronting COVID-19 Pandemics, Laboratory Investigation, 2021.

[15] M. Jiang, W. Pan, A. Arasthfer, W. Fang, L. Ling, H. Fang, F. Daneshnia, J. Yu, W. Liao, H. Pei, X. Li, C. Lass-Floerl, Development and validation of a rapid, single-step reverse transcriptase loop-mediated isothermal amplification (RT-LAMP) system potentially to Be used for reliable and high-throughput screening of COVID-19, Front. Cell. Infect. Microbiol. 10 (2020).
[16] J.J. Schellenberg, M. Ormond, Y. Keynan, Extraction-free RT-LAMP to detect SARS-CoV-2 is less sensitive but highly specific compared to standard RT-PCR in 101 samples, J. Clin. Virol. 136 (2021).
[17] J. Plantamura, A. Bousquet, M.P. Otto, C. Bigaillon, A.M. Legland, H. Delacour, P. Vest, H. Astier, E. Valero, O. Bylicki, C. Renard, S. Martin, C. Verret, E. Garnotel, V. Foissaud, A. Merens, F. Janvier, Performances, feasibility and acceptability of nasopharyngeal swab, saliva and oral-self sampling swab for the detection of severe acute respiratory syndrome coronavirus 2, Eur. J. Clin. Microbiol. Infect. Dis. 40 (2021) 2191–2198.
[18] E.L.A. Howson, S.P. Kidd, B. Armson, A. Goring, J. Sawyer, C. Cassar, D. Cross, T. Lewis, J. Hockey, S. Rivers, S. Cawthraw, A. Banyard, P. Anderson, S. Rahou, M. Andreou, N. Morant, D. Clark, C. Walsh, S. Laxman, R. Houghton, J. Slater-Jefferies, P. Costello, I. Brown, N. Cortes, K.M. Godfrey, V.L. Fowler, Preliminary optimisation of a simplified sample preparation method to permit direct detection of SARS-CoV-2 within saliva samples using reverse-transcription loop-mediated isothermal amplification (RT-LAMP), J. Virol Methods 289 (2021).
[19] A. Khemka, M. Arora, A. Dave, P. Saluja, R. Rai, Saliva as a potential diagnostic tool for SARS-CoV-2, J. Evol. Med. Dental Sci. Jemds 10 (2021) 2029–2033.
[20] K.K.W. To, O.T.Y. Tsang, C.C.Y. Yip, K.H. Chan, T.C. Wu, J.M.C. Chan, W.S. Leung, T.S.H. Chik, C.Y.C. Choi, D.H. Kandamby, D.C. Lung, A.R. Tam, R.W.S. Poon, A.Y.F. Fung, I.F.N. Hung, V.C.C. Cheng, J.F.W. Chan, K.Y. Yuen, Consistent detection of 2019 novel coronavirus in saliva, Clin. Infect. Dis. 71 (2020) 841–843.
[21] P. Harikrishnan, Saliva as a potential diagnostic specimen for COVID-19 testing, J. Craniofac. Surg. 31 (2020) E653–E655.
[22] K.K.W. To, O.T.Y. Tsang, W.S. Leung, A.R. Tam, T.C. Wu, D.C. Lung, C.C.Y. Yip, J.P. Cai, J.M.C. Chan, T.S.H. Chik, D.P.L. Lau, C.Y.C. Choi, L.L. Chen, W.M. Chan, K.H. Chan, J.D. Ip, A.C.K. Ng, R.W.S. Poon, C.T. Luo, V.C.C. Cheng, J.F.W. Chan, I.F.N. Hung, Z.W. Chen, H.L. Chen, K.Y. Yuen, Temporal profiles of viral load in posterior oropharyngeal saliva samples and serum antibody responses during infection by SARS-CoV-2: an observational cohort study, Lancet Infect. Dis. 20 (2020) 565–574.
[23] C. Liu, Q.X. Shi, M.F. Peng, R.Y. Lu, H.H. Li, Y.Y. Cai, J.X. Chen, J.Q. Xu, B. Shen, Evaluation of droplet digital PCR for quantification of SARS-CoV-2 Virus in discharged COVID-19 patients, Aging-Us 12 (2020) 20997–21003.
[24] A. David, L. Scott, S. Jugwanth, M. Gededzha, T. Kahamba, N. Zwane, N. Mampeule, I. Sanne, W. Stevens, E.S. Mayne, Operational characteristics of 30 lateral flow immunoassays used to identify COVID-19 immune response, J. Immunol. Methods (2021) 496.
[25] J. Dinnes, J.J. Deeks, S. Berhane, M. Taylor, A. Adriano, C. Davenport, S. Dittrich, D. Emperador, Y. Takwoingi, J. Cunningham, S. Beese, J. Domen, J. Dretzke, L.F. di Ruffano, I.M. Harris, M.J. Price, S. Taylor-Phillips, L. Hooft, M.M.G. Leeflang, M.D. McInnes, R. Spijker, A. Van den Bruel, C.-D.T.A. Cochrane, Rapid, Point-Of-Care Antigen and Molecular-Based Tests for Diagnosis of SARS-CoV-2 Infection, Cochrane Database of Systematic Reviews, 2021.
[26] M. Garcia-Finana, D.M. Hughes, C.P. Cheyne, G. Burnside, M. Stockbridge, T.A. Fowler, V.L. Fowler, M.H. Wilcox, M.G. Semple, I. Buchan, Performance of the Innova SARS-CoV-2 antigen rapid lateral flow test in the Liverpool asymptomatic testing pilot: population based cohort study, BMJ Br. Med. J. (Clin. Res. Ed.) (2021) 374.
[27] T. Peto, C.-L.F.O. Uk, COVID-19: rapid antigen detection for SARS-CoV-2 by lateral flow assay: a national systematic evaluation of sensitivity and specificity for mass-testing, Eclinicalmedicine 36 (2021).
[28] E. Schuit, I.K. Veldhuijzen, R.P. Venekamp, W. van den Bijllaardt, S.D. Pas, E.B. Lodder, R. Molenkamp, C.H. GeurtsvanKessel, J. Velzing, R.C. Huisman, L. Brouwer, T.L. Boelsums, G.J. Sips, K.S.M. Benschop, L. Hooft, J.H.H.M. van de Wijgert, S. van den Hof, K.G.M. Moons, Diagnostic accuracy of rapid antigen tests in asymptomatic and presymptomatic close contacts of individuals with confirmed SARS-CoV-2 infection: cross sectional study, BMJ Br. Med. J. (Clin. Res. Ed.) 374 (2021).
[29] N.M. Bergmann, N.A. Peppas, Molecularly imprinted polymers with specific recognition for macromolecules and proteins, Prog. Polym. Sci. 33 (2008) 271–288.
[30] D. Stevenson, H.F. El-Sharif, S.M. Reddy, Selective extraction of proteins and other macromolecules from biological samples using molecular imprinted polymers, Bioanalysis 8 (2016) 2255–2263.
[31] M. Gast, H. Sobek, B. Mizaikoff, Advances in imprinting strategies for selective virus recognition a review, Trac. Trends Anal. Chem. 114 (2019) 218–232.
[32] A.A. Malik, C. Nantasenamat, T. Piacham, Molecularly imprinted polymer for human viral pathogen detection, Mater. Sci. Eng. C Mater. Biol. Appl. 77 (2017) 1341–1348.
[33] M.V. Sullivan, S.R. Dennison, G. Archontis, S.M. Reddy, J.M. Hayes, Toward rational design of selective molecularly imprinted polymers (MIPs) for proteins: computational and experimental studies of acrylamide based polymers for myoglobin, J. Phys. Chem. B 123 (2019) 5432–5443.
[34] S.P. Graham, H.F. El-Sharif, S. Hussain, R. Fruengel, R.K. McLean, P.C. Hawes, M.V. Sullivan, S.M. Reddy, Evaluation of molecularly imprinted polymers as synthetic virus neutralizing antibody mimics, Front. Bioeng. Biotechnol. 7 (2019).
[35] O.I. Parisi, M. Dattilo, F. Patitucci, R. Malivindi, S. Delbue, P. Ferrante, S. Parapini, R. Galeazzi, M. Cavarelli, F. Cilurzo, S. Franze, I. Perrotta, V. Pezzi, F. Selmin, M. Ruffo, F. Puoci, Design and development of plastic antibodies against SARS-CoV-2 RBD based on molecularly imprinted polymers that inhibit in vitro virus infection, Nanoscale 13 (40) (2021) 16885–16899.
[36] A. Bossi, F. Bonini, A.P.F. Turner, S.A. Piletsky, Molecularly imprinted polymers for the recognition of proteins: the state of the art, Biosens. Bioelectron. 22 (2007) 1131–1137.
[37] R. Gui, H. Jin, H. Guo, Z. Wang, Recent advances and future prospects in molecularly imprinted polymers-based electrochemical biosensors, Biosens. Bioelectron. 100 (2018) 56–70.
[38] V.V. Shumyantseva, T.V. Bulko, I.H. Baychorov, A.I. Archakov, Molecularly imprinted polymers (MIP) in electroanalysis of proteins, Biochem Moscow Suppl. B Biomed. Chem. 10 (2016) 145–151.
[39] L. Bueno, H.F. El-Sharif, M.O. Salles, R.D. Boehm, R.J. Narayan, T. Paixao, S.M. Reddy, MIP-based electrochemical protein profiling, Sensor. Actuator. B Chem. 204 (2014) 88–95.
[40] M.V. Sullivan, W.J. Stockburn, P.C. Hawes, T. Mercer, S.M. Reddy, Green synthesis as a simple and rapid route to protein modified magnetic nanoparticles for use in the development of a fluorometric molecularly imprinted polymer-based assay for detection of myoglobin, Nanotechnology 32 (2021).
[41] J. Erdossy, V. Horvath, A. Yarman, F.W. Scheller, R.E. Gyurcsanyi, Electrosynthesized molecularly imprinted polymers for protein recognition, Trac. Trends Anal. Chem. 79 (2016) 179–190.
[42] F.T.C. Moreira, R.A.F. Dutra, J.P.C. Noronha, M.G.F. Sales, Electrochemical biosensor based on biomimetic material for myoglobin detection, Electrochim. Acta 107 (2013) 481–487.
[43] N. Taheri, H. Khoshsafar, M. Ghanei, A. Ghazvini, H. Bagheri, Dual-template rectangular nanotube molecularly imprinted polypyrrole for label-free impedimetric sensing of AFP and CEA as lung cancer biomarkers, Talanta (2022) 239.
[44] A. Raziq, A. Kidakova, R. Boroznjak, J. Reut, A. Opik, V. Syritski, Development of a Portable MIP-Based Electrochemical Sensor for Detection of SARS-CoV-2 Antigen, vol. 178, Biosensors & Bioelectronics, 2021.
[45] J. Bu, Z. Deng, H. Liu, J. Li, D. Wang, Y. Yang, S. Zhong, Current Methods and Prospects of Coronavirus Detection, Talanta, 2021, p. 225.
[46] R. Jalandra, A.K. Yadav, D. Verma, N. Dalal, M. Sharma, R. Singh, A. Kumar, P.R. Solanki, Strategies and perspectives to develop SARS-CoV-2 detection methods and diagnostics, Biomed. Pharmacother. 129 (2020).
[47] M.A. Tabrizi, J.P. Fernandez-Blazquez, D.M. Medina, P. Acedo, An Ultrasensitive Molecularly Imprinted Polymer-Based Electrochemical Sensor for the Determination of SARS-CoV-2-RBD by Using Macroporous Gold Screen-Printed Electrode, vol. 196, Biosensors & Bioelectronics, 2022.
[48] A.G. Ayankojo, R. Boroznjak, J. Reut, A. Opik, V. Syritski, Molecularly imprinted polymer based electrochemical sensor for quantitative detection of SARS-CoV-2 spike protein, Sensor. Actuator. B Chem. 353 (2022).
[49] S.A. Hashemi, S. Bahrani, S.M. Mousavi, N. Omidifar, N.G.G. Behbahan, M. Arjmand, S. Ramakrishna, K.B. Lankarani, M. Moghadami, M. Firoozsani, Graphene-based femtogram-level sensitive molecularly imprinted polymer of SARS-CoV-2, Adv. Mater. Interfac. 8 (2021).
[50] C. Conceicao, N. Thakur, S. Human, J.T. Kelly, L. Logan, D. Bialy, S. Bhat, P. Stevenson-Leggett, A.K. Zagrajek, P. Hollinghurst, M. Varga, C. Tsirigoti, M. Tully, C. Chiu, K. Moffat, A.P. Silesian, J.A. Hammond, H.J. Maier, E. Bickerton, H. Shelton, I. Dietrich, S.C. Graham, D. Bailey, The SARS-CoV-2 Spike protein has a broad tropism for mammalian ACE2 proteins, PLoS Biol. 18 (2020).
[51] N. Thakur, G. Gallo, A.M.E. Elreafey, D. Bailey, Production of recombinant replication-defective lentiviruses bearing the SARS-CoV or SARS-CoV-2 attachment spike glycoprotein and their application in receptor tropism and neutralisation assays, Bio-Protocol 11 (2021).
[52] J. ter Meulen, E.N. van den Brink, L.L.M. Poon, W.E. Marissen, C.S.W. Leung, F. Cox, C.Y. Cheung, A.Q. Bakker, J.A. Bogaards, E. van Deventer, W. Preiser, H.W. Doerr, V.T. Chow, J. de Kruif, J.S.M. Peiris, J. Goudsmit, Human monoclonal antibody combination against SARS coronavirus: synergy and coverage of escape mutants, PLoS Med. 3 (2006) 1071–1079.
[53] J.D. Huo, Y.G. Zhao, J.S. Ren, D.M. Zhou, H.M.E. Duyvesteyn, H.M. Ginn, L. Carrique, T. Malinauskas, R.R. Ruza, P.N.M. Shah, T.K. Tan, P. Rijal, N. Coombes, K.R. Bewley, J.A. Tree, J. Radecke, N.G. Paterson, P. Supasa, J. Mongkolsapaya, G.R. Screaton, M. Carroll, A. Townsend, E.E. Fry, R.J. Owens, D.I. Stuart, Neutralization of SARS-CoV-2 by destruction of the prefusion spike, Cell Host Microbe 28 (2020) 445. -+.
[54] H.F. El-Sharif, D. Stevenson, S.M. Reddy, MIP-based protein profiling: a method for interspecies discrimination, Sensor. Actuator. B Chem. 241 (2017) 33–39.
[55] H.F. El-Sharif, N.W. Turner, S.M. Reddy, M.V. Sullivan, Application of Thymine-Based Nucleobase-Modified Acrylamide as a Functional Co-monomer in Electropolymerised Thin-Film Molecularly Imprinted Polymer (MIP) for Selective Protein (Haemoglobin) Binding, Talanta, 2021, p. 123158.
[56] H.F. El-Sharif, Q.T. Phan, S.M. Reddy, Enhanced selectivity of hydrogel-based molecularly imprinted polymers (HydroMIPs) following buffer conditioning, Anal. Chim. Acta 809 (2014) 155–161.
[57] D.M. Hawkins, D. Stevenson, S.M. Reddy, Investigation of protein imprinting in hydrogel-based molecularly imprinted polymers (HydroMIPs), Anal. Chim. Acta 542 (2005) 61–65.

[58] J. Fajnzylber, J. Regan, K. Coxen, H. Corry, C. Wong, A. Rosenthal, D. Worrall, F. Giguel, A. Piechocka-Trocha, C. Atyeo, S. Fischinger, A. Chan, K.T. Flaherty, K. Hall, M. Dougan, E.T. Ryan, E. Gillespie, R. Chishti, Y. Li, N. Jilg, D. Hanidziar, R.M. Baron, L. Baden, A.M. Tsibris, K.A. Armstrong, D.R. Kuritzkes, G. Alter, B.D. Walker, X. Yu, J.Z. Li, P. Massachusetts Consortium, SARS-CoV-2 viral load is associated with increased disease severity and mortality, Nat. Commun. 11 (2020).

[59] H.F. El-Sharif, D.M. Hawkins, D. Stevenson, S.M. Reddy, Determination of protein binding affinities within hydrogel-based molecularly imprinted polymers (HydroMIPs), Phys. Chem. Chem. Phys. 16 (2014) 15483–15489.